REPORT ON THE UPDATED HECO ANALYSIS

Laura Patrizii and James Pinfold

MENU

1. *Major Corrections:*
    1. *More background material*
    2. *Updated MMT Material*
    3. *More material on NTDs eg false positives, scanning details, etc*
    4. *New material on systematic errors in NTDs*
    5. *Bugs found in original calculations (due to hardwired normalization/multiplier + another bug) – giving rise to updated results*
    6. *The Conclusion*

BACKGROUND MATERIAL

Some changes to the introductory Material including a new figure

charge, μ_0 is the permeability of free space and n is an integer.

The DQC indicates that if the magnetic charge exists then the electric charge is quantized in units of $e = 2\pi\hbar/(\mu_0)g_D$. The value of g_D is approximately 68.5e. Dirac's theory did not constrain the mass or the spin of the monopole. Further, the Dirac quantization condition indicates a coupling strength much bigger than one: $\alpha_m = \mu_0 g_D^2/(4\pi\hbar c) \approx 34$. Thus, perturbation theory cannot be applied and cross-section calculations based on perturbation theory are not physically valid, although useful as a benchmark.

In 1974 't Hooft [20] and Polyakov [21] discovered monopole solutions of the non-Abelian Georgi-Glashow model [22]. This model has only one gauge symmetry, SO(3), with a three component Higgs field. The mass of the 't Hooft-Polyakov MM was predicted to be around 100 GeV. However, MMs with such a low mass were ruled out by experiment. Subsequently, Georgi and Glashow combined their electroweak theory with a theoretical description of strong nuclear forces to form a Grand Unified Theory (GUT) [23] using the single non-Abelian gauge symmetry, SU(5). In this GUT theory the MM would have a mass of $\sim 10^{15}$ GeV which is far too heavy to be directly produced at any foreseeable terrestrial collider.

Although the Standard Model has an $SU(2) \times U(1)$ group structure that does not allow a finite-energy monopole, Cho and co-workers have modified its structure to admit the possibility of an "electroweak" monopole [24, 25] with a magnetic charge of $2g_D$. Based on this work Cho, Kim and Yoon (CKY) [26] have more recently presented an adaptation of the Standard Model - including a non-minimal coupling of its Higgs field to the square of its U(1) gauge coupling strength - that permits the possibility of a finite energy dyon [27].

The question of whether it is possible to create generalizations of the CKY model that are consistent with the Standard Model was considered by Ellis, Mavromatos and You (EMY) [28]. EMY concluded that there is a possibility that an "electroweak" monopole, consistent with the current constraints on the Standard Model, may exist and be detectable at the LHC. The existence of a MM is such a theoretically well predicated and revolutionary possibility that the search for a MM has been carried out as each new energy frontier is broached.

We consider here only those models that admit a magnetic charge quantized in units of Dirac charge, g_D, or a multiple of the Dirac charge. As $g_D = 68.5e$, a relativistic monopole with a single Dirac charge will ionize $\sim$4700

holes [33].

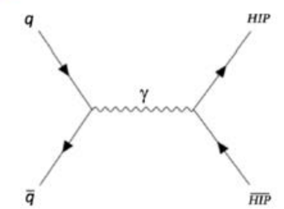

FIG. 1. Tree level Feynman diagram for DY production of HIP anti-HIP pairs.

The first searches for MMs and/or HECOs at the LHC were performed by the ATLAS and MoEDAL Collaborations in 8 TeV p-p collisions [4, 5, 8]. At this stage, the ATLAS monopole search was sensitive to singly magnetically charged ($1g_D$) monopoles, whereas the MoEDAL search was sensitive to single and multiply charged monopoles. ATLAS and MoEDAL continued the quest for HIPs at RUN2.

In the case of MMs, the ATLAS and MoEDAL searches were complementary, in the sense that ATLAS utilized the MMs highly ionizing signature [7, 14] whereas, until now, the MoEDAL experiment only exploited the induction technique to directly detect the magnetic charge [9–11]. Extensive accelerator searches for HECOs at the LHC have also been undertaken [4, 6, 7, 14]. The latest result from LHC describes the ATLAS experiment search for HECOs and monopoles using data taken during LHC's Run-2 at a centre-of-mass energy of 13 TeV [15].

In this paper we report the first use of the prototype MoEDAL Nuclear Track Detector (NTD) System, which relies on an ionization signal to detect HIPs in conjunction with the prototype MoEDAL trapping detector system that utilizes a Superconducting Quantum Interference Device (SQUID) to detect the presence of trapped magnetic charge. The complete prototype detector is shown in Figure 2. A total of 2.2 fb^{-1} of $p-p$ collision data was obtained during LHC's Run-1 at LHC intersection point IP8 on the LHC ring using this detector and analyzed for evidence of HECOs.

A DY mechanism provides a simple model for HIP pair production. Both HECO pair production and monopole

pair production cross sections are computed using the Feynman-like diagrams shown in Figure 1. It should be noted that the large monopole-photon coupling places such calculations in the non-perturbative regime.

MORE ON THE MMT DETECTOR

A small amount of material more on the MMT detector plus a new figure

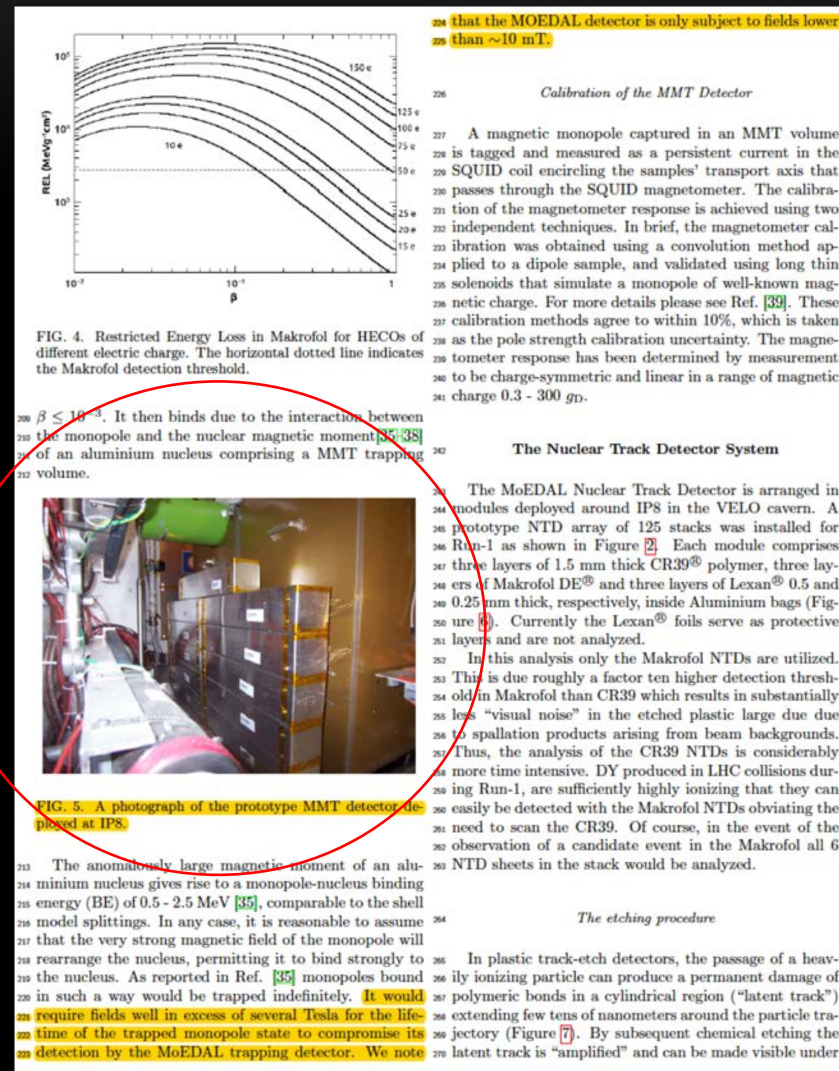

FIG. 4. Restricted Energy Loss in Makrofol for HECOs of different electric charge. The horizontal dotted line indicates the Makrofol detection threshold.

$\beta \leq 10^{-3}$. It then binds due to the interaction between the monopole and the nuclear magnetic moment [35–38] of an aluminium nucleus comprising a MMT trapping volume.

FIG. 5. A photograph of the prototype MMT detector deployed at IP8.

The anomalously large magnetic moment of an aluminium nucleus gives rise to a monopole-nucleus binding energy (BE) of 0.5 - 2.5 MeV [35], comparable to the shell model splittings. In any case, it is reasonable to assume that the very strong magnetic field of the monopole will rearrange the nucleus, permitting it to bind strongly to the nucleus. As reported in Ref. [35] monopoles bound in such a way would be trapped indefinitely. It would require fields well in excess of several Tesla for the lifetime of the trapped monopole state to compromise its detection by the MoEDAL trapping detector. We note that the MOEDAL detector is only subject to fields lower than ~10 mT.

Calibration of the MMT Detector

A magnetic monopole captured in an MMT volume is tagged and measured as a persistent current in the SQUID coil encircling the samples' transport axis that passes through the SQUID magnetometer. The calibration of the magnetometer response is achieved using two independent techniques. In brief, the magnetometer calibration was obtained using a convolution method applied to a dipole sample, and validated using long thin solenoids that simulate a monopole of well-known magnetic charge. For more details please see Ref. [39]. These calibration methods agree to within 10%, which is taken as the pole strength calibration uncertainty. The magnetometer response has been determined by measurement to be charge-symmetric and linear in a range of magnetic charge 0.3 - 300 g_D.

The Nuclear Track Detector System

The MoEDAL Nuclear Track Detector is arranged in modules deployed around IP8 in the VELO cavern. A prototype NTD array of 125 stacks was installed for Run-1 as shown in Figure 2. Each module comprises three layers of 1.5 mm thick CR39® polymer, three layers of Makrofol DE® and three layers of Lexan® 0.5 and 0.25 mm thick, respectively, inside Aluminium bags (Figure 6). Currently the Lexan® foils serve as protective layers and are not analyzed.

In this analysis only the Makrofol NTDs are utilized. This is due roughly a factor ten higher detection threshold in Makrofol than CR39 which results in substantially less "visual noise" in the etched plastic large due due to spallation products arising from beam backgrounds. Thus, the analysis of the CR39 NTDs is considerably more time intensive. DY produced in LHC collisions during Run-1, are sufficiently highly ionizing that they can easily be detected with the Makrofol NTDs obviating the need to scan the CR39. Of course, in the event of the observation of a candidate event in the Makrofol all 6 NTD sheets in the stack would be analyzed.

The etching procedure

In plastic track-etch detectors, the passage of a heavily ionizing particle can produce a permanent damage of polymeric bonds in a cylindrical region ("latent track") extending few tens of nanometers around the particle trajectory (Figure 7). By subsequent chemical etching the latent track is "amplified" and can be made visible under

MORE MATERIAL ON NTDS (1)

Efficiency and False Positives for NTD detectors

middle layer would be etched and analyzed. However, no candidate was found.

If no candidates were found in the first Makrofol foil in a stack, no other foils would be scanned. However, the CR39 foils all stacks are retained for future analyses, where the the REL threshold is much lower, roughly ten times less than Makrofol.

The Detection Threshold for Makrofol

For the HIP to be detected its REL must be greater than the detection threshold of the Makrofol. The detection threshold will vary with the etching conditions. It will also vary with the angle of incidence of the HIP (δ) on the NTD. The connection between the threshold and the maximum angle of incidence (δ_{Max}) to the normal to the NTD that the HIP can make and still be detected, is expressed by the relationship: $p = \frac{1}{cos(\delta_{Max})}$. Everything else being equal, the greater the maximum angle of incidence the lower the detection threshold. The lowest threshold is obtained for a HIP impinging normally to the NTD. The curve showing the relation between δ_{Max} and the REL is shown in Figure 11.

Efficiency and False Positives in the NTD Detectors

As described above the signal for the passage of a HIP messenger of new physics passing through a MoEDAL NTD stack would be a string of etch pits in the stack, where an etch pit pair is due to the ingress and egress of the HIP passing though an NTD sheet. No such signal has ever been seen in this search, or by any other HIP search employing NTDs [2]. Indeed, no candidates, or false positives as they would be classified as candidate, were seen in the 125 stacks examined (corresponding to 7.8 m^2), where only the most upstream sheet of the NTD stacks were examined.

The absence of false positives using the NTD technique is borne out by the astroparticle physics experiments MACRO [46] and SLIM [47] , which deployed a surface area of 1263 m^2 and 427 m^2, respectively, and did not observe a single HIP candidate. It should be noted that the NTD technique employed by these experiments are essentially identical to those employed at colliders.

The lack of false positives in the NTD technique at colliders or in astroparticle physics experiment raises the question of the false negatives, or detector efficiency. This can be evaluated using the heavy ion beams that are used to calibrate NTD detectors. In the absence of beam backgrounds, the detection, or scanning, efficiency for the etch pits due to heavy-ion HIPs with ionizing power above the NTD threshold was measured to be in excess of 99%.

In order to estimate the effect of beam background on the detection efficiency of NTDs for HIPs we utilized NTD calibration stacks exposed to a relativistic lead-ion beam as described above. The stacks were comprised of sheets of Makrofol NTDs exposed to the beam backgrounds in the VELO cavern at the LHC for a year of data taking interleaved with unexposed Makrofol NTD sheets. Plastic from the same production batch was used in calibration and standard data taking.

The NTDs sheets comprising the calibration stacks were then etched in the same way as the standard NTD stacks deployed for data taking during Run-1. The individual sheets were then scanned using the same manually controlled optical scanning microscope technology employed to examine all MoEDAL NTD stacks. The relativistic lead-ion calibration beam particles penetrate

8

the whole stack allowing the signal etch pits seen in the plastic sheet that was not previously exposed to the LHC beam - where the signal can clearly be observed with a 100% efficiency - to serve as a map. This map can be used to assess the efficiency of the scan of the adjacent NTD sheet that had been exposed to LHC beam backgrounds. These studies, indicate that the efficiency for detection above threshold was in excess of 99%. This number was determined by multiple scanning of the same sheets by different scanners.

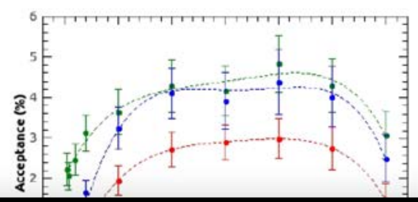

MORE MATERIAL ON NTDS (2)

The acceptance is better explained

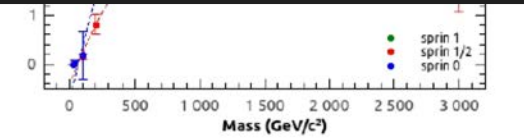

FIG. 13. Acceptance for monopole pair production with magnetic charge $2g_D$.

ACCEPTANCE OF THE RUN-1 MOEDAL DETECTOR

The MoEDAL detector's acceptance is defined to be the fraction of the number of events in which at least one HIP of the Drell-Yan (DY) produced pair was detected in MoEDAL in either the NTD detector or the MMT detector. The acceptance for DY production of HECOs and magnetic monopoles is described by an interplay of the geometrical disposition of MoEDAL NTD modules and MMT detectors, energy loss in the detectors, mass of the particle and the spin-dependent kinematics of the interaction products. In the case of the HECOs, MoEDAL's NTD system provides the only means of detection.

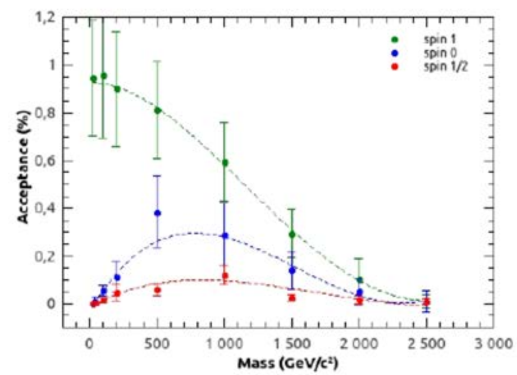

FIG. 12. Acceptance for spin-1, spin-0 and spin-1/2 HECOs with charge 125e.

For a given HIP mass and charge, the pair-production model determines the kinematics and the overall trapping acceptance obtained. The uncertainty in the acceptance is dominated by uncertainties in the material description [8–10]. This contribution is estimated by performing simulations with hypothetical material conservatively added and removed from the nominal geometry model. An example, showing the MoEDAL NTD acceptance curves for spin-1/2, spin-0, spin-1 HECOs with charge 125e is shown in Figure 12. The acceptance curves for spin-0, spin-1/2 and spin-1 monopoles, found using the NTD and MMT detectors combined, are shown in Figure 13. The corresponding curves for spin-0 and spin-1 monopoles follow the same general form. The acceptance for $1g_D$ rises roughly quadratically to a maximum around 2.5 TeV of nearly 11% to 12% for both spin-0 and spin-1 monopoles. For $2g_D$, the acceptance curves reach a plateau between ∼500 GeV and 2.5 TeV, of approximately 4%. The curves for $3g_D$ follow the same form as does that of $2g_D$, but the plateau is only ∼2%. For 4 and $5g_D$ the acceptance reaches a very broad maximum at less than 1% before falling to zero at 3 TeV. The acceptances shown in Figure 12 and Figure 13 refer to the prototype detector deployed for LHC's Run-1.

ANALYSIS RESULTS

The first Makrofol sheet of each of MoEDAL's 125 NTD stacks, exposed during LHC's Run-1 were etched and scanned, as described above, for evidence of the passage through the sheet of a highly ionizing object such as a HECO or a magnetic monopole. The total area of plastic analyzed was 7.8 m^2 (Run-1). No candidate events were observed. In addition, no monopole candidates were observed to be trapped in the MMT detector. This is the first time that the data from the MoEDAL prototype detector, deployed during Run-1, has been presented.

There are two dominant sources of systematic error in this analysis. The first arises from the imperfect knowledge of the amount of material between the interaction

MORE MATERIAL ON NTDS (3)

Extra material on the etching and calibration process

FIG. 6. NTD module composition

an optical microscope. In the etching process, the bulk of the material is removed at a rate v_B and at a higher rate v_T along the latent track. The damage zone is revealed under an optical microscope as a cone shaped etch–pit, called "track". Etch–pits surface openings have a circular shape for normally incident particles, otherwise they are elliptical.

A sketch of an etch-pit at different etching times is shown in Figure 7 for a normally incident particle crossing the detector with a constant energy loss. Two etching conditions were applied (Table I). The first was the so-called "strong" etching [40] condition, allowing faster etching and yielding larger etch-pits that were easier to detect under visual scanning. Strong etching was applied to the first, most upstream, Makrofol foil in each module. The second, "soft etching", condition results in a slower etching process. This allows the etching process to proceed in several steps in order to follow the formation of etch-pits. Soft etching is applied to subsequent Makrofol foils in the stack, if a candidate track is found in the first layer. In Figure 8 are shown microphotographs of relativistic Pb^{82+} tracks in Makrofol foils etched in (left) "soft conditions"; (right) "strong conditions".

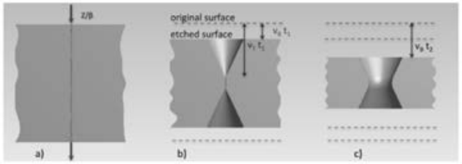

FIG. 7. Illustration of the track-etch technique: a) latent track forming along the trajectory of a high ionizing particle impinging perpendicularly on the NTD surface ; b) development of conical pits during the etching process; c) etch-pits joining after a prolonged etching, forming a hole in the detector.

Pb^{82+} and 13 A GeV Xe^{54+} ion beams at the CERN SPS. The calibration set-up included a stack of Makrofol foils placed upstream and downstream of an Aluminum target. Incoming ions undergo charge changing nuclear fragmentation interaction along their path through the detector foils and the target. After exposure the detectors were etched in 6N KOH+20% ethyl alcohol at 50 °C for 10 hours. The bulk etch velocity was $v_B = 3.4\ \mu m/h$.

After etching, the size of surface tracks was measured with an automatic scanning system providing the cone base area, and the coordinates of the center of the etch pits. Etch pits diameters typically range from 10 μm to 100 μm, with a modal value in the range 30 μm to 40 μm. The base area distributions of incoming ions and of their fragments is shown in Fig. 9. The projectile fragments have the same velocity and approximately the same direction as the incident ions. From the base area spectrum, the charge corresponding to each nuclear fragment peak can be identified, and the corresponding REL determined. A detailed description of the calibration procedure can be found in [41].

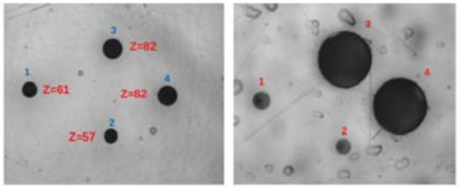

FIG. 8. Microphotographs of relativistic Pb^{82+} tracks and of nuclear fragments (Z<82) in two consecutive foils of Makrofol. Each image frame measures 0.64 mm x 0.80 mm. Etch pits are from the same ions crossing the detector foils: (left) Makrofol foil etched in "soft conditions"; (right) Makrofol foil etched in "strong conditions". Note that the microphotographs also show two clearly differentiated fragmentation products of Pb: La (Z = 57); and, Pm (Z=61).

For each identified peak the reduced etch rate p, the Z/β and eventually the restricted energy loss are computed (Fig.9). Calibration data thus obtained are shown in Fig.10. The mimimum detectable relativistic charge is $Z/\beta \geq 50$, both in soft or strong etching. The detector threshold is at REL ~ 2700 MeV $g^{-1}cm^2$.

NTDs are detection threshold devices. In CR39 and in

SYSTEMATIC ERRORS ON NTD MEASUREMENT (1)

First Version

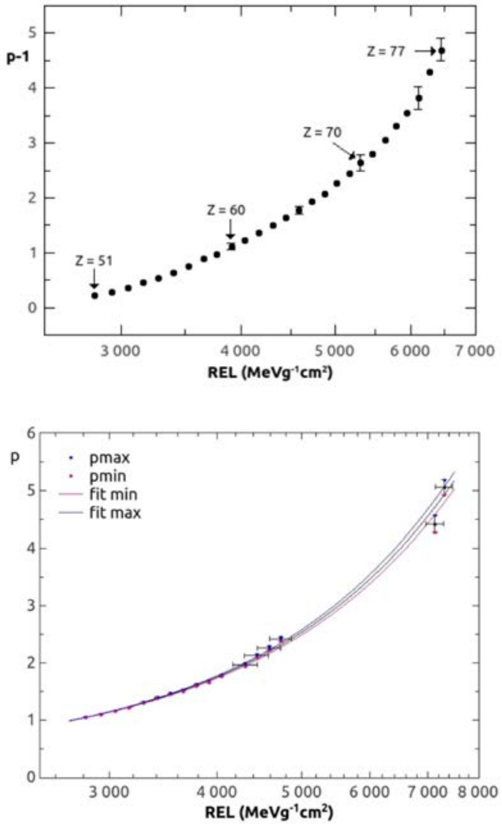

FIG. 10. Reduced etch-rate versus REL for Makrofol exposed to relativistic Lead and Xenon ion beams: (top) detectors etched in soft conditions;(bottom) detectors etched in strong conditions. The upper and low curves are drawn through the $\pm 1\sigma$ value of the error on each p value, where the error bars represent a convolution of the statistical and systematic error on each point.

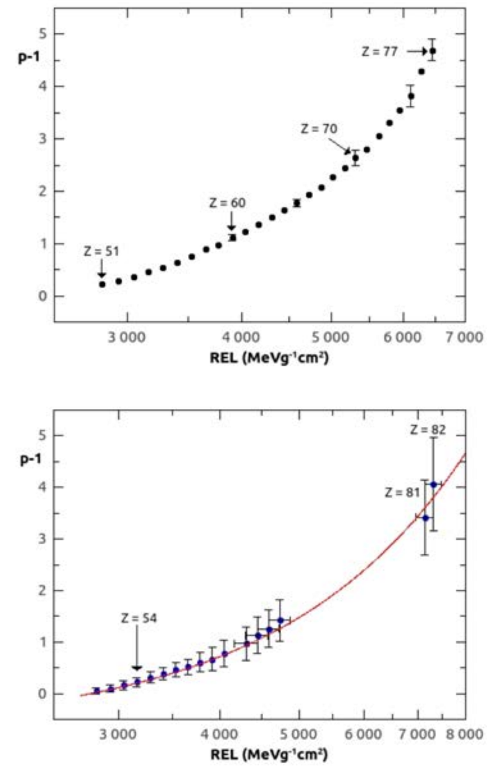

FIG. 8. Reduced etch-rate versus REL for Makrofol exposed to relativistic Lead and Xenon ion beams: (top) detectors etched in soft conditions;(bottom) detectors etched in strong conditions.

SYSTEMATIC ERRORS ON NTD MEASUREMENT (2)

8.0 radiation lengths (X_0) in thickness and on average around 1.4 X_0 [42] thick. The main contribution to the systematic uncertainty in this analysis arises from the estimate of the material in the GEANT4 geometry description. The uncertainty in the material map is modelled by two geometries which represent an excess and a deficit of material, using conservative estimates of uncertainties on material thicknesses and densities, compared to the best assessment of the material budget that is compatible with direct measurement and existing drawings.

This systematic uncertainty in the material map gives rise to uncertainties in the DY acceptances. For singly charge monopoles ($|g| = g_D$) the resulting relative uncertainty is of the order of 10% [8]. This uncertainty increases with electric and magnetic charge. For a doubly charged monopoles ($|g| = 2g_D$) it is of the order of 10 - 20% for intermediate masses, around 1 TeV.

Other sources of systematic error are an uncertainty due to a conservative estimate of 1 cm uncertainty in the trapping detector position. Simulations show this error lies in the range 1-17% [8]. Another source of systematics is the uncertainty in dE/dx as a function of β, resulting in a 1-10% relative uncertainty in the acceptance [8].

In the case of monopoles and HECOS a systematic error on the variable p, due to the NTD etching and calibration process is given in Figure 10 (bottom). This error on p can give rise to an error on the threshold value for detection of the plastic as well as an error on the variation of efficiency with angle of the NTD. However, these uncertainties are negligible compared to the error on the material map discussed above. All of the above sources of systematic error were added in quadrature and included in the final limit calculation.

We calculated the 95% C.L. upper limits to the cross-section using as a measure a Drell–Yan model for HECO and magnetic monopole production assuming a $\beta-$independent monopole coupling and that the monopole can have a spin of $0, 1/2$ and 1. The limit curves obtained are shown in Figure 14 for HECOs. For monopoles the cross section upper limits versus mass are given in Figure 15 for spin $0, 1/2$ and 1. The values of the 95% C.L. mass limits are listed in Table II and Table III, for HECOs and magnetic monopoles, respectively.

CONCLUSIONS

Both MoEDAL's prototype NTD system and aluminium elements of the MoEDAL MMT detector, were exposed to 8 TeV LHC collisions during LHC's Run-1. At the end of Run-1 both detector systems were examined for the presence of magnetic monopoles and/or HECOs. The NTDs were etched and scanned to reveal evidence for the passage of a magnetic monopole or a HECO using semi-automatic and manual optical microscopes. In the case of the MMT a SQUID-based magnetometer was

MORE MATERIAL ON NTDS (3)

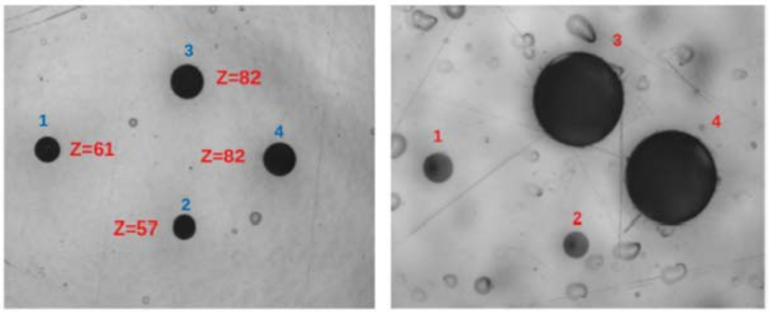

FIG. 8. Microphotographs of relativistic Pb^{82+} tracks and of nuclear fragments (Z<82) in two consecutive foils of Makrofol. Each image frame measures 0.64 mm x 0.80 mm. Etch pits are from the same ions crossing the detector foils: (left) Makrofol foil etched in "soft conditions"; (right) Makrofol foil etched in "strong conditions". Note that the microphotographs also show two clearly differentiated fragmentation products of Pb: La (Z = 57); and, Pm (Z=61).

FIRST VERSION

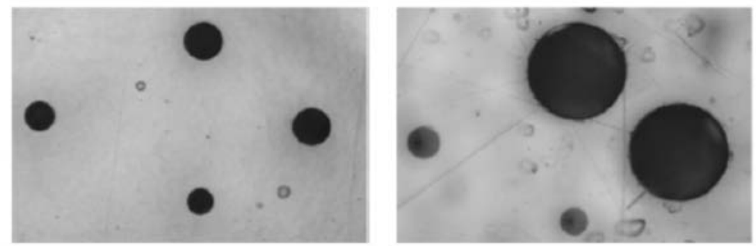

FIG. 6. Microphotographs of relativistic Pb^{82+} tracks and of nuclear fragments (Z<82) in two consecutive foils of Makrofol. Each image frame measures 0.64 mm x 0.80 mm. Etch pits are from the same ions crossing the detector foils: (left) Makrofol foil etched in "soft conditions"; (right) Makrofol foil etched in "strong conditions".

NEW LIMITS

A search for highly electrically charged objects (HECOs) and magnetic monopoles is presented using 2.2 fb^{-1} of p-p collision data taken at a centre of mass energy (E_{CM}) of 8 TeV by the MoEDAL detector during LHC's Run-1. The data were collected using MoEDAL's prototype Nuclear Track Detector array and the Trapping Detector array. The results are interpreted in terms of Drell-Yan pair production of stable HECO and monopole pairs with three spin hypotheses (0, 1/2 and 1). The search provides constraints on the direct production of magnetic monopoles carrying one to four Dirac magnetic charges ($4g_D$) and with mass limits ranging from 590 GeV to 1 TeV. Additionally, mass limits are placed on HECOs with charge in the range $10e$ to $180e$, where e is the charge of an electron, for masses between 30 GeV and 1 TeV.

TABLE II. 95% CL mass limits for the HECO search corrected.

	Electric charge (e)														
	10	15	20	25	50	75	100	125	130	140	145	150	160	170	180
Spin	95% CL mass limits [GeV]														
0	30	110	220	270	560	560	540	500	500	470	470	450	400	-	-
1/2	100	270	420	550	770	760	700	600	590	560	550	-	-	-	-
1	-	360	550	700	1010	1020	1000	960	940	920	910	890	870	850	840

TABLE III. 95% CL mass limits for the magnetic monopole search.

	Magnetic charge (g_D)			
	1	2	3	4
Spin	95% CL mass limits [GeV]			
0	590	740	710	520
1/2	910	1090	1020	700
1	1030	1190	1190	1110

FIRST VERSION

A search for highly electrically charged objects (HECOs) and magnetic monopoles is presented using 2.2 fb^{-1} of p-p collision data taken at a centre of mass energy of 8 TeV by the MoEDAL detector during LHC's Run-1. The data were collected using MoEDAL's Nuclear Track Detector array and the Trapping Detector array. The results are interpreted in terms of Drell–Yan pair production of stable HECO and monople pairs with three spin hypotheses (0, 1/2 and 1). The search provides constraints on the direct production of magnetic monopoles carrying one to five Dirac magnetic charges ($5g_D$) and with mass limits ranging from 710 GeV to 1230 GeV. Additionally, mass limits are placed on HECOs with charge in the range $10e$ to $165e$, where e is the charge of an electron, for masses between 640 GeV and 2000 GeV.

TABLE II. 95% CL mass limits for the HECO search.

	Electric charge/e													
	10	15	20	25	50	75	100	125	130	140	145	150	160	165
Spin	95% CL mass limits [GeV]													
0	640	950	1190	1350	1530	1500	1430	1360	1330	1310	1290	1280	1270	1260
1/2	1090	1450	1650	1770	1840	1750	1650	1520	1470	1480	1490	1450	-	-
1	1100	1440	1670	1840	2000	1960	1900	1800	1780	-	-	-	-	-

TABLE III. 95% CL mass limits for the magnetic monopole search.

	magnetic charge/g_D				
	1	2	3	4	5
Spin	95% CL mass limits [GeV]				
0	710	780	740	530	-
1/2	990	1090	1020	-	-
1	1150	1230	1210	1120	950

THE CONCLUSION

The conclusion has changed in detail.

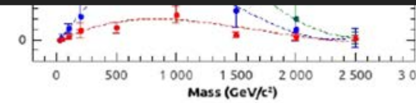

FIG. 12. Acceptance for spin-1, spin-0 and spin-1/2 HECOs with charge 125e.

For a given HIP mass and charge, the pair-production model determines the kinematics and the overall trapping acceptance obtained. The uncertainty in the acceptance is dominated by uncertainties in the material description [8–10]. This contribution is estimated by performing simulations with hypothetical material conservatively added and removed from the nominal geometry model. An example, showing the MoEDAL NTD ac-

ANALYSIS RESULTS

The first Makrofol sheet of each of MoEDAL's 125 NTD stacks, exposed during LHC's Run-1 were etched and scanned, as described above, for evidence of the passage through the sheet of a highly ionizing object such as a HECO or a magnetic monopole. The total area of plastic analyzed was 7.8 m^2 (Run-1). No candidate events were observed. In addition, no monopole candidates were observed to be trapped in the MMT detector. This is the first time that the data from the MoEDAL prototype detector, deployed during Run-1, has been presented.

There are two dominant sources of systematic error in this analysis. The first arises from the imperfect knowledge of the amount of material between the interaction point and the MoEDAL NTD modules, due to LHCb's VELO detector. The VELO vacuum vessel and the various elements of the VELO detector with LHCb's acceptance are simulated with great precision in the LHCb geometry. However, detailed technical drawings of other elements of VELO upstream of the sensitive elements of VELO such as cables, in-situ electronics, cooling pipes, various flanges, a vacuum pump and a vacuum manifold, are not available.

Nominally, this intervening material is between 0.1 and 8.0 radiation lengths (X_0) in thickness and on average around 1.4 X_0 [42] thick. The main contribution to the systematic uncertainty in this analysis arises from the estimate of the material in the GEANT4 geometry description. The uncertainty in the material map is modelled by two geometries which represent an excess and a deficit of material, using conservative estimates of uncertainties on material thicknesses and densities, compared to the best assessment of the material budget that is compatible with direct measurement and existing drawings.

This systematic uncertainty in the material map gives rise to uncertainties in the DY acceptances. For singly charge monopoles ($|g| = g_D$) the resulting relative uncertainty is of the order of 10% [8]. This uncertainty increases with electric and magnetic charge. For a doubly charged monopoles ($|g| = 2g_D$) it is of the order of 10 - 20% for intermediate masses, around 1 TeV.

Other sources of systematic error are an uncertainty due to a conservative estimate of 1 cm uncertainty in the trapping detector position. Simulations show this error lies in the range 1-17% [8]. Another source of systematics is the uncertainty in dE/dx as a function of β, resulting in a 1-10% relative uncertainty in the acceptance [8].

In the case of monopoles and HECOS a systematic error on the variable p, due to the NTD etching and calibration process is given in Figure 10 (bottom). This error on p can give rise to an error on the threshold value for detection of the plastic as well as an error on the variation of efficiency with angle of the NTD. However, these uncertainties are negligible compared to the error on the material map discussed above. All of the above sources of systematic error were added in quadrature and included in the final limit calculation.

We calculated the 95% C.L. upper limits to the cross-section using as a measure a Drell–Yan model for HECO and magnetic monopole production assuming a β−independent monopole coupling and that the monopole can have a spin of $0, 1/2$ and 1. The limit curves obtained are shown in Figure 14 for HECOs. For monopoles the cross section upper limits versus mass are given in Figure 15 for spin $0, 1/2$ and 1. The values of the 95% C.L. mass limits are listed in Table II and Table III, for HECOs and magnetic monopoles, respectively.

CONCLUSIONS

Both MoEDAL's prototype NTD system and aluminium elements of the MoEDAL MMT detector, were exposed to 8 TeV LHC collisions during LHC's Run-1. At the end of Run-1 both detector systems were examined for the presence of magnetic monopoles and/or HECOs. The NTDs were etched and scanned to reveal evidence for the passage of a magnetic monopole or a HECO using semi-automatic and manual optical microscopes. In the case of the MMT a SQUID-based magnetometer was